




# Application of honeybee venom loaded nanoparticles for the treatment of chronic toxoplasmosis: parasitological, histopathological, and immunohistochemical studies

Heba M. El Naggar<sup>1</sup> · Mona M Anwar<sup>1</sup> · Amira E. Khayyal<sup>1</sup> · Reda M Abdelhameed<sup>2</sup> · Ashraf M. Barakat<sup>3</sup> · Sabry A. S. Sadek<sup>3</sup> · Ayman M. Elashkar<sup>1,4</sup> 

Received: 2 January 2023 / Accepted: 27 May 2023 / Published online: 7 June 2023  
© Indian Society for Parasitology 2023

## Abstract

*Toxoplasma gondii* is an opportunistic intracellular protozoon which may cause severe disease in the immunocompromised patients. Unfortunately, the majority of treatments on the market work against tachyzoites in the acute infection but can't affect tissue cysts in the chronic phase. So, this study aimed to evaluate the effect of bee venom (BV) loaded metal organic frameworks (MOFs) nanoparticles (NPs) for the treatment of chronic murine toxoplasmosis. Ninety laboratory Swiss Albino mice were divided into 9 groups (10 mice each); GI (negative control), GII (infected control), GIII–GXII (infected with Me49 strain of *Toxoplasma* and treated); GIII (MOFs-NPs), GIV and GV (BV alone and loaded on MOFs-NPs), GVI and GVII (spiramycin alone and loaded on MOFs-NPs), GVIII and GIX (ciprofloxacin alone and loaded on MOFs-NPs). Parasitological examination of brain cyst count, histopathological study of brain, retina, liver, and kidney tissue sections and immunohistochemical (IHC) evaluation of liver was performed. Counting of *Toxoplasma* brain cysts showed high statistically significant difference between the infected treated groups and GII. GV showed the least count of brain cysts; mean  $\pm$  SD ( $281 \pm 29.5$ ). Histopathological examination revealed a marked ameliorative effect of BV administration when used alone or loaded MOFs-NPs. It significantly reduced tissue inflammation, degeneration, and fibrosis. IHC examination of liver sections revealed high density CD8<sup>+</sup> infiltration in GII, low density CD8<sup>+</sup> infiltration in GIII, GVI, GVII, GVIII, and GIX while GIV and GV showed intermediate density CD8<sup>+</sup> infiltration. BV is a promising Apitherapy against chronic toxoplasmosis. This effect is markedly enhanced by MOFs-NPs.

✉ Ayman M. Elashkar  
aymanpara@yahoo.com

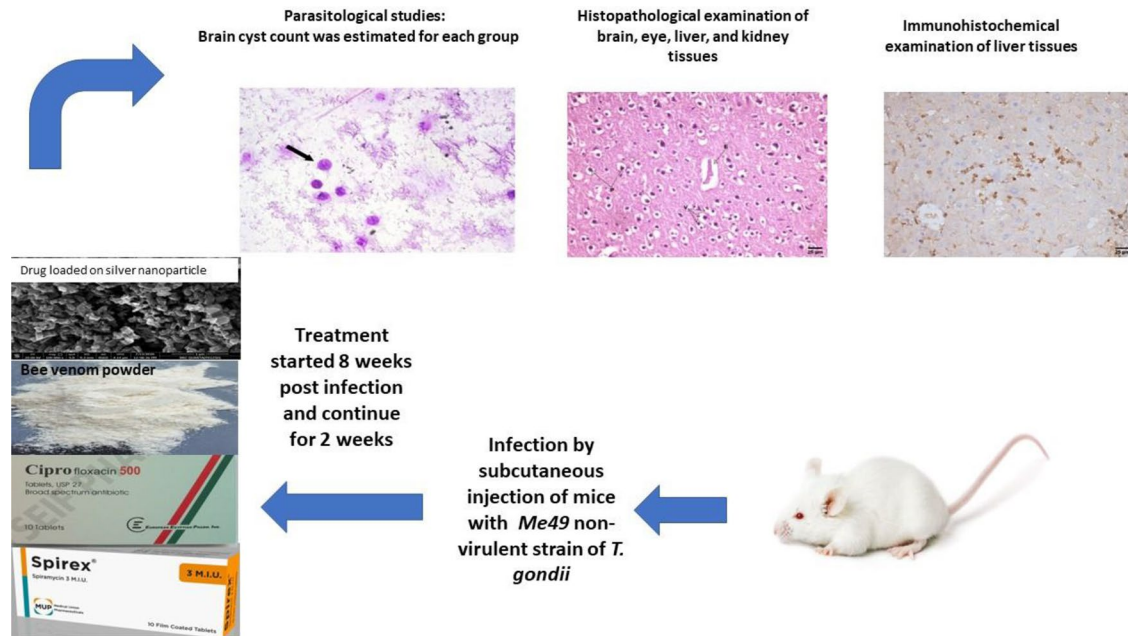
<sup>1</sup> Department of Medical Parasitology, Faculty of Medicine, Ain Shams University, Cairo, Egypt

<sup>2</sup> Department of Applied Organic Chemistry, Chemical Industries Research Division, National Research Centre, Giza, Egypt

<sup>3</sup> Department of Zoonotic Diseases, National Research Centre, Giza, Egypt

<sup>4</sup> Department of Basic Medical Sciences, College of Medicine, University of Bisha, Bisha, KSA, Saudi Arabia

## Graphical abstract



**Keywords** Bee venom · Ciprofloxacin · Metal organic frameworks · Spiramycin · Toxoplasmosis

## Introduction

The protozoan *Toxoplasma gondii* (*T. gondii*) is the culprit behind the common parasite disease toxoplasmosis, which affects human populations. The parasite infects about two billion people globally, and its epidemiological distribution varies by region depending on geography, climatic conditions, eating patterns, the history of keeping cats as pets, literacy levels, and cleanliness standards (Rayani et al. 2020; Omidian et al. 2022).

Immunocompromised individuals are at a significant mortality risk from the prevalent opportunistic infection toxoplasmosis, typically due to reactivation of infection in the central nervous system, even though it typically only causes mild disease in healthy individuals (Matta et al. 2021). *Toxoplasma* infections are believed to infect around 30% of humans, causing a fatal illness in the immunodeficient, and HIV/AIDS was the most common co-occurring condition with *Toxoplasma* infections (Shammaa et al. 2021). Immune responses depending on interferon regulate the rapid parasite proliferation during the acute phase of infection. However, after spreading, the parasite divides into cysts that grow inside muscle cells and neurons and remain there for the rest of the infected host's life (Matta et al. 2021). Congenital toxoplasmosis continues to be a major source of illness and mortality on a global scale. In about 40% of cases, pregnant women who contract *T.*

*gondii* during pregnancy can pass the parasite to the foetus causing abortion or foetal abnormalities (CDC 2020).

Despite serious side effects being documented, the combined therapy of pyrimethamine and sulphadiazine that targets the folate pathway continues to be the gold standard for the treatment of *Toxoplasma* infections (Shammaa et al. 2021). Besides, treating asymptomatic toxoplasmosis and infection in pregnant females, spiramycin and azithromycin are the most widely used drugs but unfortunately, spiramycin has low bioavailability and poor penetration of the blood brain barrier. So, *Toxoplasma* encephalitis is treated with combination of pyrimethamine and sulphadiazine, or pyrimethamine and clindamycin, or clindamycin and atovaquone. Using these drug combinations for long period may cause serious adverse reactions (Wei et al. 2015). Moreover, ciprofloxacin was proved to be effective against acute toxoplasmosis and its efficacy was enhanced by loading on silver NPs (Ahmed et al. 2022). Nevertheless, ciprofloxacin was proved to elevate the danger of preterm labour, abortion, and fetal anomalies (Ziv et al. 2018; Acar et al. 2019). Moreover, because the available medications only work against tachyzoites and not bradyzoites, they are unable to remove tissue cysts from infected hosts, which are dormant in immunocompetent people for their whole lives and become reactivated in immunocompromised patients (El-Shafey et al. 2020).

Apitherapy is a complementary therapy that uses honeybee products, most significantly bee venom (BV), to treat a variety of human illnesses. Humans have employed honeybee products including honey, propolis, and venom from the European honeybee *Apis mellifera* (*A. mellifera*) as medicines for thousands of years (Khalil et al. 2021).

Bee venom is typically associated with discomfort since bee stings can result in localized irritation and potentially an allergic reaction in humans. Traditional applications of BV include acupuncture and traditional Chinese medicine. It is made up of a variety of elements, primarily proteins and peptides, as well as enzymes and other kinds of molecules in extremely small quantities. Melittin and phospholipase A2 (PLA2) are the most prevalent and extensively researched BV substances (Carpena et al. 2020).

Melittin is a naturally occurring antimicrobial peptide that makes up between 50 and 60 percent of the dry weight (DW) of venom from the *A. mellifera*, making it the component that is more prevalent in BV. Melittin is also the molecule with the widest range of biological activities that have been seen, as well as important clinical and therapeutic effects; despite this, it is the most poisonous component of the BV (Pucca et al. 2020). According to Adade et al., treatment with crude *A. mellifera* venom causes a range of cell death patterns in treated parasites and is fatal to *Trypanosoma cruzi* (*T. cruzi*), the cause of Chagas disease (Adade et al. 2013).

The enzyme phospholipase A2 (PLA2), which makes up around 10–12% of BV, is the second substance more prevalent and the second substance with the most biological activity (Abd El-Wahed et al. 2018). Moreira et al. directed the antiparasitic effector genes to create transgenic *Anopheles stephensi* mosquitoes that express the PLA2 gene from BV. Importantly, transgenic expression of PLA2 protein in mosquito intestine significantly hindered *Plasmodium berghei* transmission to uninfected mice by reducing oocyst development by an average of 87% (Moreira et al. 2002). On the other hand, PLA2 is the most allergenic component of BV causing allergenic sensitization in 57–97% of allergic people (Jakob et al. 2017).

Peptides such apamin, mast cell-degranulation peptide (MCD), secapin, and adolapin, as well as enzymes like hyaluronidase, are additional elements that are only weakly present in BV yet exhibit substantial physiologic functions. Apamin is a neurotoxic peptide composed of 18 amino acids and has the ability to inhibit the Ca<sup>2+</sup>-activated K<sup>+</sup> channel. 22 aa make up MCD, which constitutes 1% to 3% of BV. Additionally, it possesses potent anti-inflammatory properties. Secapin has three appealing biological properties: anti-elastolytic, anti-microbial, and anti-fibrinolytic (Lee et al. 2016). Adolapin is a polypeptide with analgesic and anti-inflammatory properties. Finally, hyaluronidase is seen as a spreading agent that

facilitates the penetration of the cell by other BV factors (Carpena et al. 2020).

Because BV has beneficial effects on several disorders, including musculoskeletal and neurological diseases, it is most commonly used for medicinal purposes. Today, efforts are focused on establishing safer doses and techniques along with fresh trends including creative administration methods to reduce side effects (Carpena et al. 2020). In the field of Parasitology, BV was utilized in the treatment of protozoan parasite like *Entamoeba histolytica*. As metronidazole has certain limitations such having potential mutagenesis effects in mice as well as the issue of the formation of drug-resistant species, the development of additional safer medications for amoebiasis is crucial. It was determined that oral intake of BV loaded chitosan (CS) nanoparticles can be a more effective alternative treatment for amoebiasis than BV that is injected subcutaneously (SABER et al. 2017). Saleh et al. examined the effects of BV on *Schistosoma mansoni* (*S. mansoni*) eggs in vitro. After being incubated with various BV concentrations, the eggs' % mortality, hatchability, and shape were assessed. It was discovered that BV changes the morphology of *S. mansoni* eggs. Additionally, it has been demonstrated that *S. mansoni* miracidia are killed by BV (Saleh et al. 2020).

With the ability to alter materials on an atomic scale, nanotechnology is predicted to create some new prospects for treating and preventing diseases. Nanomaterials can be valuable for both in vivo and in vitro biomedical research (Gherbawy et al. 2013).

Nanoparticles (NPs) are small materials with sizes ranging from 1 to 100 nm. Depending on their characteristics, shapes, or sizes, they can be divided into many classifications. Fullerenes, metal NPs, ceramic NPs, and polymeric NPs are various groups of NPs. Due to their large surface area and nanoscale size, NPs have distinct physical and chemical characteristics (Khan et al. 2019). The three layers that make up NPs are as follows: (a) The surface layer, (b) The core, and (c) The shell layer (Shin et al. 2016).

Metal–organic frameworks (MOFs), a subclass of highly porous materials, have a wide range of potential uses in biology and medicine (McKinlay et al. 2010). The chemical properties of MOFs can be easily tuned by changing the metal and/or the organic linker provided higher surface area leading to the higher the drug loading capacity. Furthermore, changeable pore size allows the encapsulation of a wide range of pharmaceuticals (Trotta 2019). According to reports, MOFs can be used as antibacterial agents, drug delivery systems, therapeutic composites, nanozymes, phototherapies, and to create sensors for electrochemical, fluorometric, and colorimetric assays that can identify specific infections (Quijia et al. 2022). Furthermore, MOFs as antibacterial agents are applied to lung disease-related infections (Zheng et al. 2022). Recently, a new, experimental structure

called nano-Curcumin@MOFs was used to treat chronic toxoplasmosis (El-Shafey et al. 2020).

Keeping the previous introduction in mind, this study attempted to evaluate the effect of BV loaded MOFs-NPs for the treatment of chronic murine toxoplasmosis through parasitological evaluation of brain cyst count, histopathological examination of tissues extracted from brain, eye, liver, and kidney, and immunohistochemical studies for the different animal groups.

## Materials and methods

This was an experimental study conducted at National Research Centre (NRC) during the period from November 2020 to September 2022.

### Animals

#### Animal housing

Ninety male laboratory-bred Swiss albino mice were chosen from the NRC's animal house when they were 6 weeks old and weighed between 20 and 25 g. They were kept in plastic cages (10 mice per cage) with white wood chips for bedding, commercial complete food mixture for feeding, and tap water for drinking. Lighting (12 h light/12 h dark cycle) and temperature ( $25 \pm 2$  °C) were also controlled (El Fakhry et al. 1998). To rule out any parasite infection, mice's feces were examined (Garcia and Bruckner 1997).

#### Animal groups

See Table 1.

## Parasite and experimental infection

In order to generate chronic toxoplasmosis, the Me49 non-virulent strain of *T. gondii* was repeatedly maintained by injecting Swiss albino mice with 0.1 ml of brain homogenate containing roughly 10 cysts from previously infected animals via oral administration through gastric tube containing, approximately,  $1 \times 10^2$  tissue cysts / ml every 8 weeks. The mice brains were ground with sterile pestle and mortars then diluted with saline to a concentration of  $1 \times 10^2$  cysts/ml obtaining brain cysts suspension by using haemocytometer (Djurkovic-Djakovic et al. 2002). Infection was guaranteed by finding *T. gondii* brain cysts 2 months post infection in Giemsa-stained brain homogenate.

### Drugs

- **BV:** it was purchased in the form of powder from (Mybi-ospace, San Diego California USA). BV was prepared according to (Hegazi et al. 2014). BV was given in a dose of 0.5 mg/kg through subcutaneous injection started at 8 wpi for 2 weeks (Baek et al. 2018).
- **Spiramycin (@ Spirex 3 M.I.U):** it was available as film coated tablets from (Medical Union Pharmaceuticals). Tablets were grinded then spiramycin dosage for each mouse was calculated (100 mg/kg/ day) and dissolved in 100 µl saline to be given by oral route started at 8 wpi for 2 weeks (Hagras et al. 2019).
- **Ciprofloxacin (@ Cipro floxacin 500):** it was obtained as 500 mg tablets manufactured by (European Egyptian Pharm. IND). The tablets were crushed and dissolved in distilled water to make an oral suspension. The dose used was adjusted at 100 mg/kg/day started at 8 wpi for 2 weeks (Martins-Duarte et al. 2015).

**Table 1** Animal groups of the study

Group number (10 mice each)	Group description	Designation
Group (I):	Non-infected, non-treated	Negative control
Group (II):	Infected non-treated mice	Positive control
Group (III):	Infected, treated with MOFs-NPs 100 mg/kg/day orally by gavage (Alajmi et al. 2019)*	Infected + MOFs-NPs
Group (IV):	Infected, treated with BV 0.5 mg/kg (Baek et al. 2018)*	Infected + BV
Group (V):	Infected, treated with BV loaded MOFs-NPs (BVL-MOFs-NPs)*a	Infected + BVL-MOFs-NPs
Group (VI):	Infected, treated with Spiramycin 100 mg/kg/ day (Hagras et al. 2019)*	Infected + Spiramycin
Group (VII):	Infected, treated with Spiramycin loaded MOFs-NPs (SL-MOFs-NPs)*b	Infected + SL-MOFs-NPs
Group (VIII):	Infected mice treated with Ciprofloxacin 100 mg/kg/day (Martins-Duarte et al. 2015)*	Infected + Ciprofloxacin
Group (IX):	Infected mice treated with Ciprofloxacin loaded MOFs-NPs (CL-MOFs-NPs) *c	Infected + CL-MOFs-NPs

\* The drugs were started to be given at 8 wpi for 2 weeks (Mohammad et al. 2023)

<sup>a</sup>Group (V) received the same dose as group (IV) by subcutaneous injection

<sup>b</sup>Group (VII) received the same dose as group (VI) by gavage using oesophageal tube

<sup>c</sup>Group (IX) received the same dose as group (VIII) by gavage using oesophageal tube

## Synthesis of Al-MOF

Al-BDC (Aluminum-Benzene Dicarboxylate) was created using the following procedure: 10 mL of DMF was used to dissolve 1.066 g (8 mmol) of  $\text{AlCl}_3$  and 1.328 g (8 mmol) of terephthalic acid. For 8 h, the mixture was refluxed at 125 °C. The product was washed with DMF and filtered off. The raw product was then dissolved in 400 mL of a 50/50, v/v, combination of methanol and water. The mixture was cooked for 12 h at 100 °C before being filtered, washed, and dried (Emam et al. 2019).

## Drug loading

BV, ciprofloxacin, and spiramycin were diluted in various tubes containing 100 ml of ethanol at various concentrations in order to load them into Al-BDC NPs (100–1000 ppm). Drug solutions were mixed with 1 g of Al-BDC NPs while being agitated with a magnetic stirrer at 600 rpm for 90 min at room temperature. The solution was then left undisturbed for the following day. The supernatant and precipitate were then separated from the suspension by centrifuging it at 5000 rpm for 5 min. The difference between the concentration of BV in the solution before and after drug loading was used to calculate the amount of loaded drug. The following equation was used to determine the percentage of medication loading:

Drug loading percentage equals  $[(AB)/A] \times 100$ , where A and B stand for the initial and final drug concentration of the drug solution (Sun et al. 2013).

## Characterization of MOFs

Using X-ray diffraction (XRD) patterns on prepared materials (Cu K monochromate was employed; X'Pert MPD Philips diffractometer), the phase purity and crystallinity were determined. Transmission electron microscope and scanning electron microscope were used to examine the nanostructure morphology of MOFs (SEM: Hitachi SU-70, JP) (Abdelhameed et al. 2016).

## Parasitological examination

Ten weeks post infection (wpi), all mice were sacrificed by euthanasia through decapitation (Boivin et al. 2016). Each harvested brain was positioned on its ventral surface and divided longitudinally into two halves; one for parasitological count of brain cysts and the other half was fixed in 10% formalin for histopathological examination after staining with Haematoxylin and eosin (H&E).

Each brain sample was rinsed with sterile saline solution, followed by homogenization. Then, a glass slide was coated with 50 ul of brain homogenate, which was then air dried,

fixed with methanol, further air dried, stained for 30 min with 10% Giemsa stain, rinsed with water, and allowed to dry at room temperature. With the aid of DPX mounting solution, coverslips were secured. Finally, using a compound microscope, the cysts were counted, the number of cysts in each brain was computed, and the mean for each group was then determined (Chew et al. 2012; Eteawa et al. 2018).

$$\text{Number of brain cysts/ml} = \frac{\text{Number of cysts in 50 ul (0.05 ml)}}{0.05}$$

Number of brain cyst in the whole brain = brain cyst /ml x volume of brain homogenate x 2.

## Histopathological examination

At 10 wpi, ten mice from each group were sacrificed. The brain, eye, liver, and kidney were removed from the sacrificed animals, preserved in 10% buffered formalin solution, and then cut into sections. In the pathology lab of NRC, they were embedded in paraffin wax blocks that were sectioned, then stained with haematoxylin and eosin (H&E) to evaluate the pathological changes and the impact of various medications on the infected animals (Feldman and Wolfe 2014).

## Immunohistochemical examination

Using the avidin–biotin–peroxidase complex (ABC) technique, paraffin slices were mounted on positively charged slides. Mouse CD4 monoclonal antibody (Elabscience, Cat# E-AB-22098, Dil.: 1:100) and mouse CD8 monoclonal antibody (Elabscience, Cat# PA5036, Dil.: 1:50) were incubated on sections from each group before the chemicals needed for the ABC technique were added (Vectastain ABC-HRP kit, Vector laboratories). To identify antigen–antibody complexes, markers were expressed, peroxidase was used to label them, and diaminobenzidine (DAB, made by Sigma) was used to color them. Instead of the primary or secondary antibodies, non-immune serum was used as a negative control. Using an Olympus microscope, IHC stained slices were investigated (BX-53).

## Statistical analysis

AVOVA, Post HOC Tukey test were used for data analysis. Significance of P-value was considered if  $< 0.05$ .

## Ethical approval

All experiment was performed in according to the institutional guidelines of the NRC's Animal Research Committee with protocol approval number: 1479102021.

## Result

### Characterization of MOFs-NPs

Figure 1 shows the PXRD patterns of Al-BDC, and Al-BDC after drug loading. Drug-modified Al-MOFs exhibited similar PXRD patterns to that of Al-MIL-53, which indicates that the drug-modified Al-MOFs have been

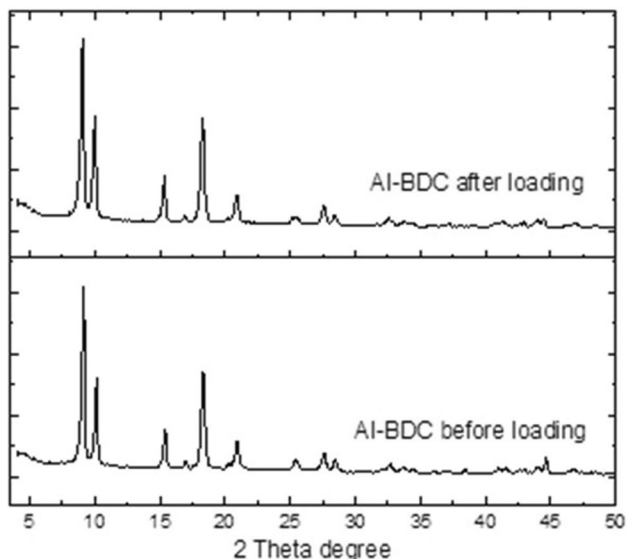


Fig. 1 PXRD patterns of Al-BDC before and after loading

synthesized successfully and they exhibit the same  $2\theta$  at  $8.5^\circ$ ,  $10.2^\circ$ ,  $12.4^\circ$ ,  $15.0^\circ$ ,  $17.4^\circ$ , and  $26.2^\circ$ , which are characterized by MIL-53.

The SEM images (Fig. 2) suggest that highly crystalline Al-MOFs particles were formed. It can be found that some long strips with  $5\ \mu\text{m}$  size of Al-BDC crystals were clearly visible, and most of them were an octahedral shape, which was uniformly dispersed and was not aggregation. After loading SEM analysis showed that the surface of Al-BDC seemed much rougher than that of Al-BDC before loading.

### Bee venom loading

The drug loading efficiency of Al-BDC nanoparticles has been examined. It is dependent on the concentration of drug and the ratio of Al-BDC NPs. The drug loading percentage increases with increase in these parameters. It increases and becomes constant at a particular level. The variation in drug loading with change in drug concentration is shown in (Fig. 3A). The loading amount is  $Q_m$  and it is equal  $216.6\ \text{mg/g}$ .

The variation in drug loading with change in stirring time is given in (Fig. 3B). With  $100\ \text{ppm}$  drug concentration and stirring at various times, the drug loading is found to be increases with increases the time. Maximum drug loading is obtained at  $90\ \text{min}$ .

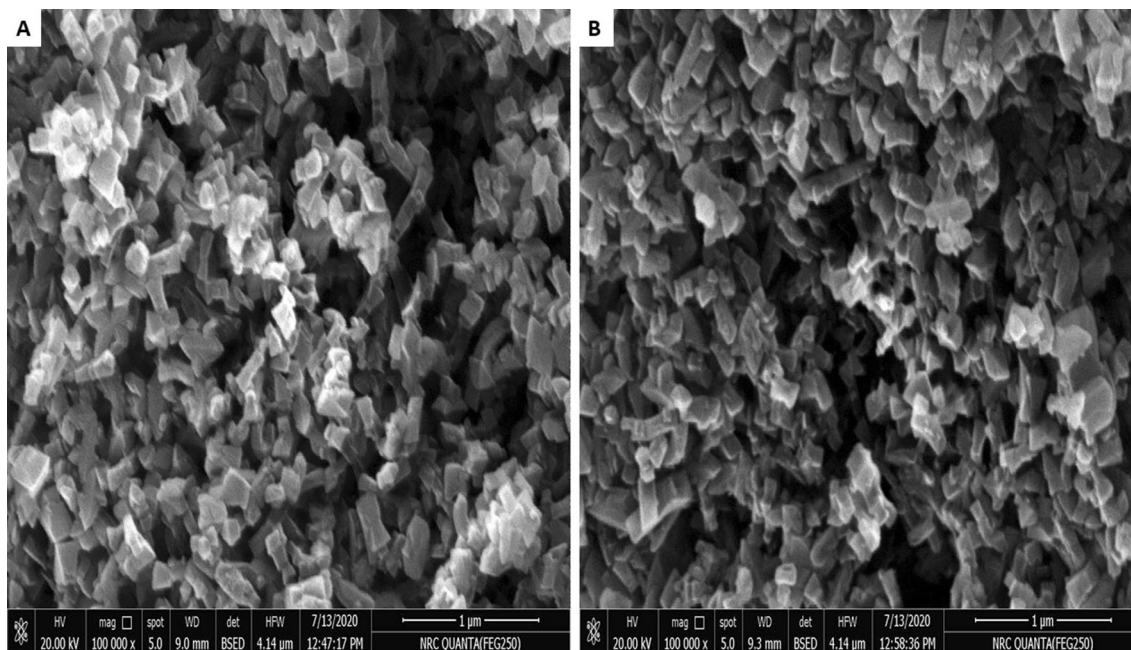
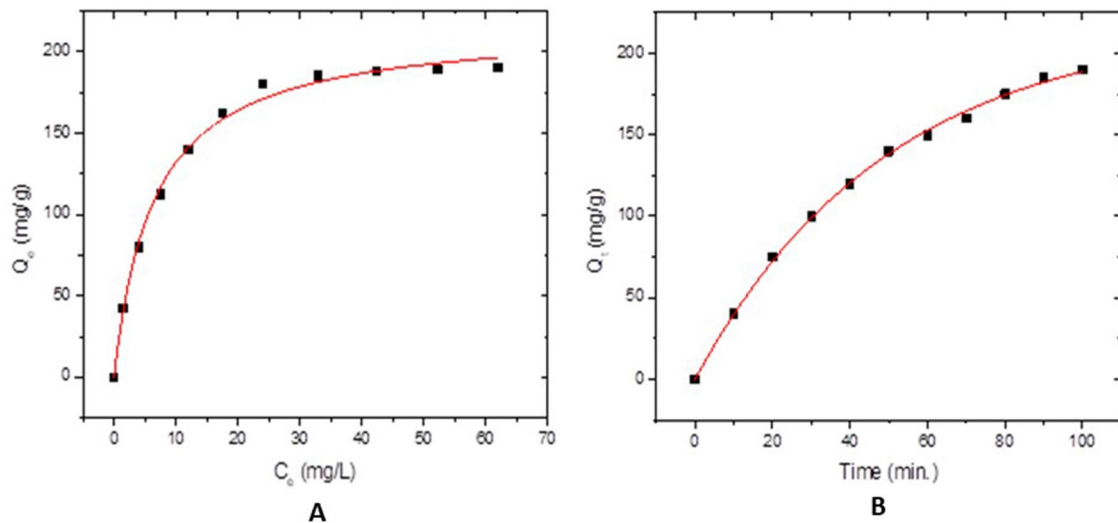


Fig. 2 Micrographs for the material; a before drug loading, b after drug loading



**Fig. 3** **A** The equilibrium between the different drug concentrations and the loading amount. **B** Effect of contact time

**Table 2** post-hoc multiple comparisons regarding brain cyst count of different study groups

Animal group (n = 10)	Brain cysts count Mean $\pm$ SD	Reduction %
GII	605 $\pm$ 36.9	
GIII	467 $\pm$ 49.5 <sup>a</sup>	22.8%
GIV	308.3 $\pm$ 3.28 <sup>ab</sup>	49%
GV	281 $\pm$ 29.5 <sup>ab</sup>	53.6%
GVI	311.5 $\pm$ 28.9 <sup>ab</sup>	48.5%
GVII	305 $\pm$ 55.8 <sup>ab</sup>	49.6%
GVIII	300.3 $\pm$ 9.61 <sup>ab</sup>	50.4%
GIX	302.43 $\pm$ 8.50 <sup>ab</sup>	50%

<sup>^</sup>ANOVA test with post-hoc Tukey HSD test

GII: Positive control; (GIII-GIX): Infected, treated with [GIII: MOF-NPs; GIV: BVL; GV: BVL-MOFs-NPs; GVI: spiramycin; GVII: SL-MOFs-NPs; GVIII: ciprofloxacin; GIX: CL-MOFs-NPs].

<sup>a</sup>Significant versus GII

<sup>b</sup>Significant versus GIII (<sup>a,b</sup> $P < 0.001$ )

## Parasitological results

Counting of *Toxoplasma* brain cysts in different study groups showed high statistically significant difference between the different infected treated groups and the infected control ( $P < 0.001$ ). GV (infected, treated with BV-NPs) showed the least count of brain cysts; mean  $\pm$  SD (281  $\pm$  29.5) although there was no statistically significant difference with the other infected treated groups (Table 2).

## Histopathological results

GI (normal control), GII (positive control); (GIII-GIX): infected, treated with [GIII: MOF-NPs; GIV: BVL; GV: BVL-MOFs-NPs; GVI: spiramycin; GVII: SL-MOFs-NPs; GVIII: ciprofloxacin; GIX: CL-MOFs-NPs].

## Brain sections

The brain sections of GI revealed normal architecture with neurons being arranged in neat rows with abundant cytoplasm, and the nuclei were round (Fig. 4a). GII showed marked histological responses in brain tissue, in the form of degeneration and distortion of neuronal architecture; other brain cells were apoptotic with vacuolated cytoplasm and pyknotic nuclei. Also, Histological staining demonstrated that the observable *T. gondii* tissue cysts were surrounded by multinucleated giant cells (Fig. 4b). GIII showed necrobiotic changes in neurons including vacuolar degeneration in cytoplasm with pyknotic nuclei and presence of axonal degeneration (Fig. 4c). GIV and GV showed improvement of brain tissue towards normal morphology as shown by regression of the total degenerative changes that were induced by infection in all brain sections. Most of neuronal cells appeared nearly normal with mild degenerative changes as vacuolization of apoptotic cells and pyknotic nuclei were observed (Fig. 4d, e). GVI and GVII showed presence of necrobiotic changes in neurons including vacuolar degeneration in cytoplasm with pyknotic nuclei, presence of axonal degeneration as well as focal gliosis in GVII (Fig. 4f, g). GVIII showed necrobiotic changes in neurons including vacuolar degeneration in cytoplasm with pyknotic nuclei and presence of axonal degeneration (Fig. 4h). GIX showed

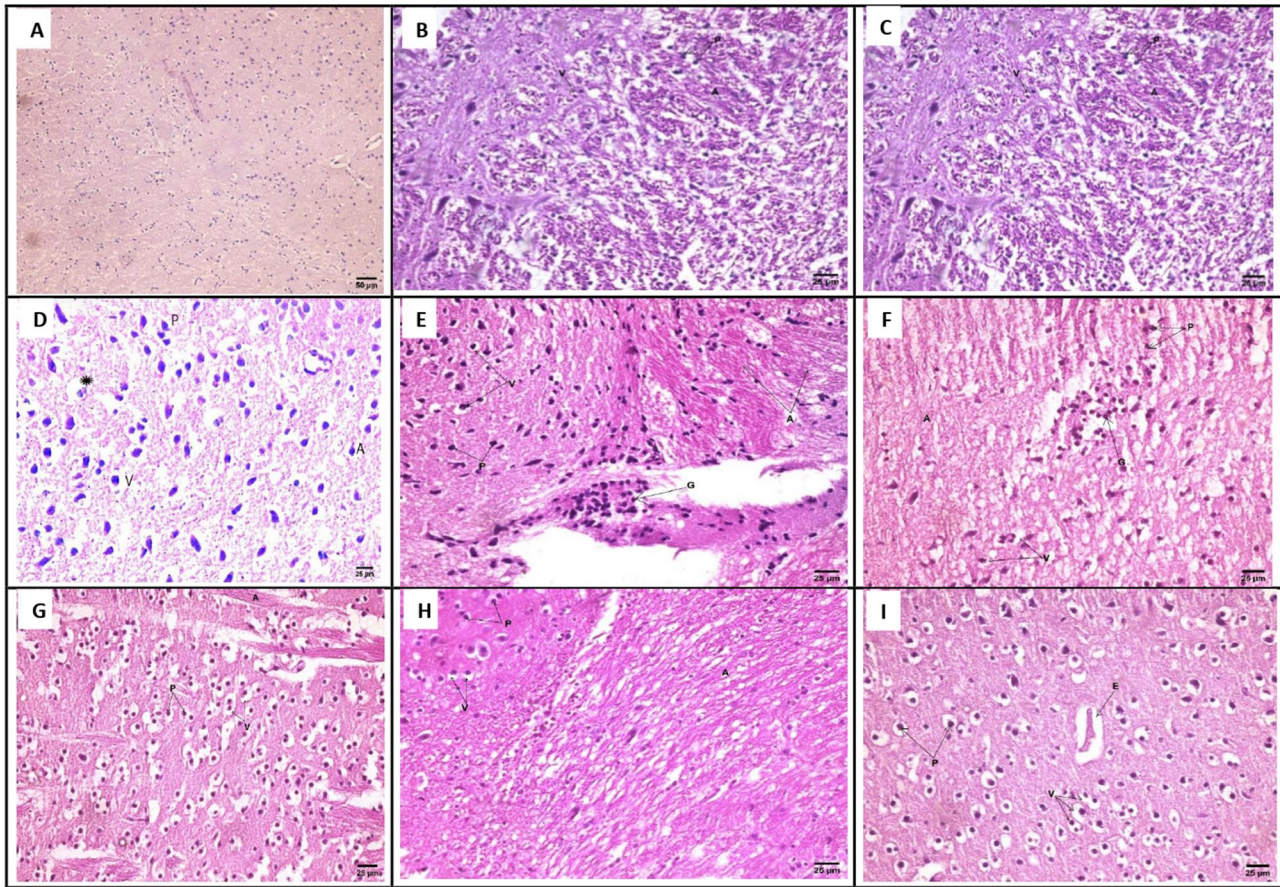


**Fig. 4** Brain sections of different study groups (Hematoxylin and Eosin, Scale bar 25 µm, ×400). **a** GI showing normal histological structure of the brain. **b** GII showing necrobiotic changes in neurons including vacuolar degeneration in cytoplasm (V) with pyknotic nuclei (P) and presence of axonal degeneration (A). **c** GIII showing necrobiotic changes in neurons including vacuolar degeneration in cytoplasm (V) with pyknotic nuclei (P) and presence of axonal degeneration (A). **d** GIV showing improvement of brain tissue with mild vacuolated cytoplasm (V), apoptotic cells (A), pyknotic nuclei (P) observable tissue cyst (star). **e** GV showing focal gliosis (G) and presence of necrobiotic changes in neurons including vacuolar degeneration in cytoplasm (V) with pyknotic nuclei (P), presence of axonal degeneration (A). **f** GVI showing focal gliosis (G) and presence of necrobiotic changes in neurons including vacuolar degeneration in

cytoplasm (V) with pyknotic nuclei (P), presence of axonal degeneration (A). **g** GVII showing necrobiotic changes in neurons including vacuolar degeneration in cytoplasm (V) with pyknotic nuclei (P) and presence of axonal degeneration (A). **h** GVIII showing necrobiotic changes in neurons including vacuolar degeneration in cytoplasm (V) with pyknotic nuclei (P) and presence of axonal degeneration (A). **i** GIX showing moderate necrobiotic changes in neurons including vacuolar degeneration in cytoplasm (V) with pyknotic nuclei (P) and presence of perivascular edema (E). [GI (normal control), GII (infected control), GIII (infected, NPs treated), GIV (infected, BV treated), GV (infected, BVL-MOFs-NPs), GVI (infected, spiramycin treated), GVII (infected, SL-MOFs-NPs), GVIII (infected, ciprofloxacin treated), GIX (infected, CL-MOFs-NPs)]

that brain tissue had moderately degenerated apoptotic cells with mild vacuolated cytoplasm and pyknotic nuclei and perivascular oedema (Fig. 4i).

### Eye sections

Histopathological examination of eye sections from GI showed normal microscopic picture of eye (Fig. 5a), from GII showed infiltration of ganglionic cell layer by few number mononuclear inflammatory cells, mild disorganization of outer nuclear layer (Photoreceptor cells) and presence of tachyzoites of *Toxoplasma* in smooth muscle

(Fig. 5b), from GIII showed infiltration of vitreous by few number of mononuclear inflammatory cells, disorganization of outer nuclear layers (Fig. 5c), from GIV showed infiltration of vitreous by few number of mononuclear inflammatory cells, disorganization of outer nuclear layers (Fig. 5d), from GV showed infiltration of ganglionic cell layer by mononuclear inflammatory cells, disorganization of inner and outer nuclear layers (photoreceptor cells) (Fig. 5e), from GVI showed disorganization of photoreceptor cell layers (Fig. 5f), from GVII, GVIII, and GIX showed disorganization of outer nuclear layers (Fig. 5g, h, and i).



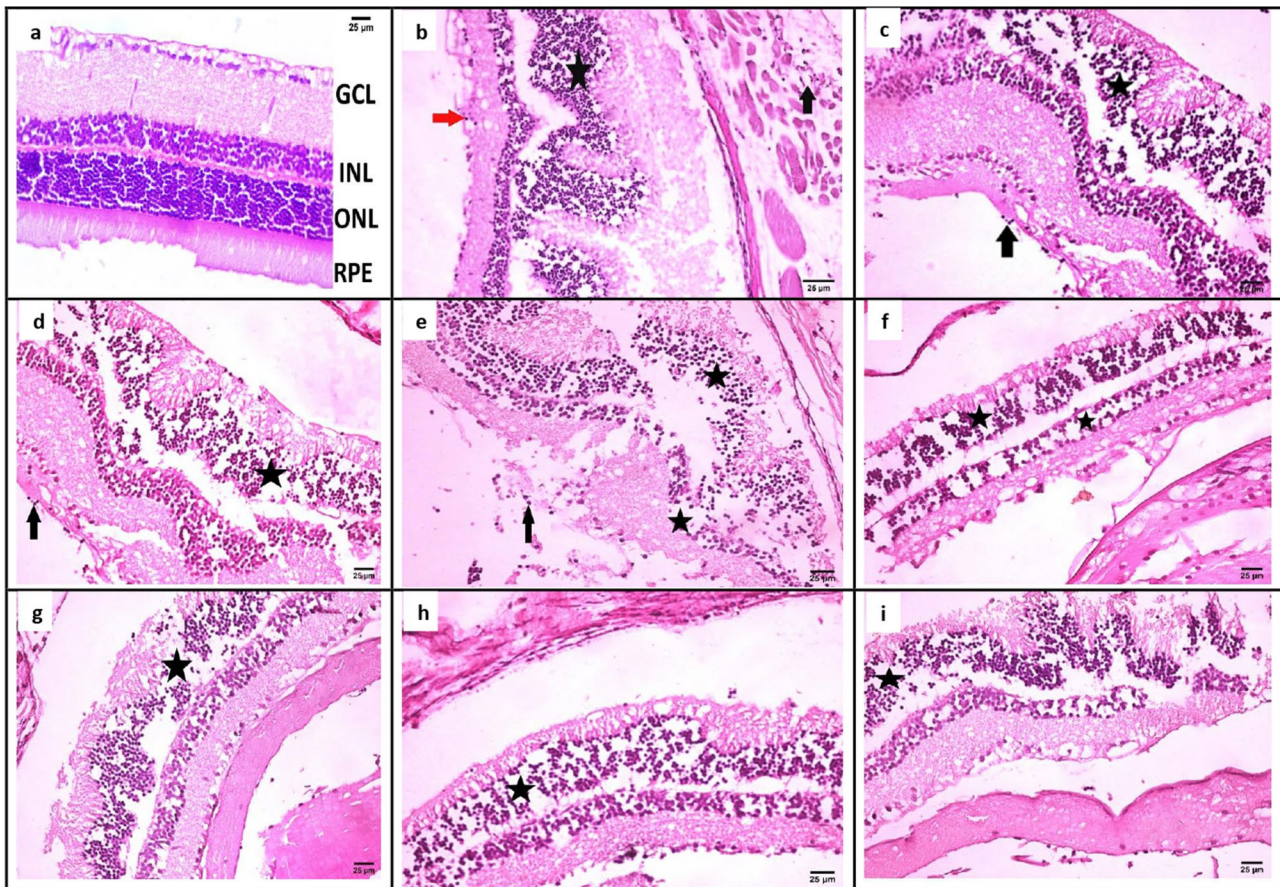


**Fig. 5** Eye sections of different study groups (Hematoxylin and Eosin, Scale bar 25  $\mu$ m, X400). **a** GI showing normal microscopic picture of retina. **b** GII showing infiltration of ganglionic cell layer by few number mononuclear inflammatory cells (red arrow), mild disorganization (star) of outer nuclear layer (Photoreceptor cells) and presence of tachyzoites of *Toxoplasma* (T) in smooth muscle (black arrow). **c** GIII showing infiltration of vitreous by few number of mononuclear inflammatory cells (black arrow), disorganization (D) of outer nuclear layers (Photoreceptor cells) (star). **d** GIV showing infiltration of vitreous by few number of mononuclear inflammatory cells (black arrow), disorganization (D) of outer nuclear layers (Photoreceptor cells) (star). **e** GV showing infiltration of ganglionic cell layer

by mononuclear inflammatory cells (arrow), disorganization (stars) of inner and outer nuclear layers (Photoreceptor cells). **f** GVI showing disorganization (stars) of inner and outer nuclear layers (Photoreceptor cells) (stars). **g** GVII showing disorganization (star) of outer nuclear layers (Photoreceptor cells). **h** GVIII showing disorganization (star) of outer nuclear layers (Photoreceptor cells). **i** GIX showing disorganization (star) of outer nuclear layers (Photoreceptor cells). [GI (normal control), GII (infected control), GIII (infected, NPs treated), GIV (infected, BV treated), GV (infected, BVL-MOFs-NPs), GVI (infected, spiramycin treated), GVII (infected, SL-MOFs-NPs), GVIII (infected, ciprofloxacin treated), GIX (infected, CL-MOFs-NPs)]

### Liver sections

Histological examination of the sections from GI revealed normal characteristics of hepatic architecture; hepatocytes arranged in cords radiating from the central veins and rounded vesicular nuclei with blood sinusoids (Fig. 6a), from GII showed hepatocytes hydropic degeneration and necrosis, focal inflammatory cell infiltration detected around central vein. Eosinophilic cytoplasm hepatocytes, enlargement of sinusoids, mild activation of Kupffer cells were also noticed with deeply stained pyknotic nuclei (Fig. 6b), from GIII, and GIV showed ameliorative effects that associated with few inflammatory cells. Moreover, enlargement of sinusoids,

and activation of Kupffer cells were found (Fig. 6c, d), from GV showed focal infiltration of mononuclear inflammatory cells between hepatocytes with activation of von kupffer cells and some hepatocytes showing pyknotic nuclei, from GVI, GVIII, microscopic investigation showed degenerative liver cells that associated with mild necrosis, and inflammatory cell infiltration around central vein. On the other hand, pyknotic nuclei, enlargement of sinusoids, mild activation of Kupffer cells were noticed (Fig. 6f, h), from GVII revealed focal infiltration of mononuclear inflammatory cells between hepatocytes and some hepatocytes showing pyknotic nuclei (Fig. 6g), from GIX showed necrobiotic changes in some hepatocytes, presence of pyknotic nuclei in others

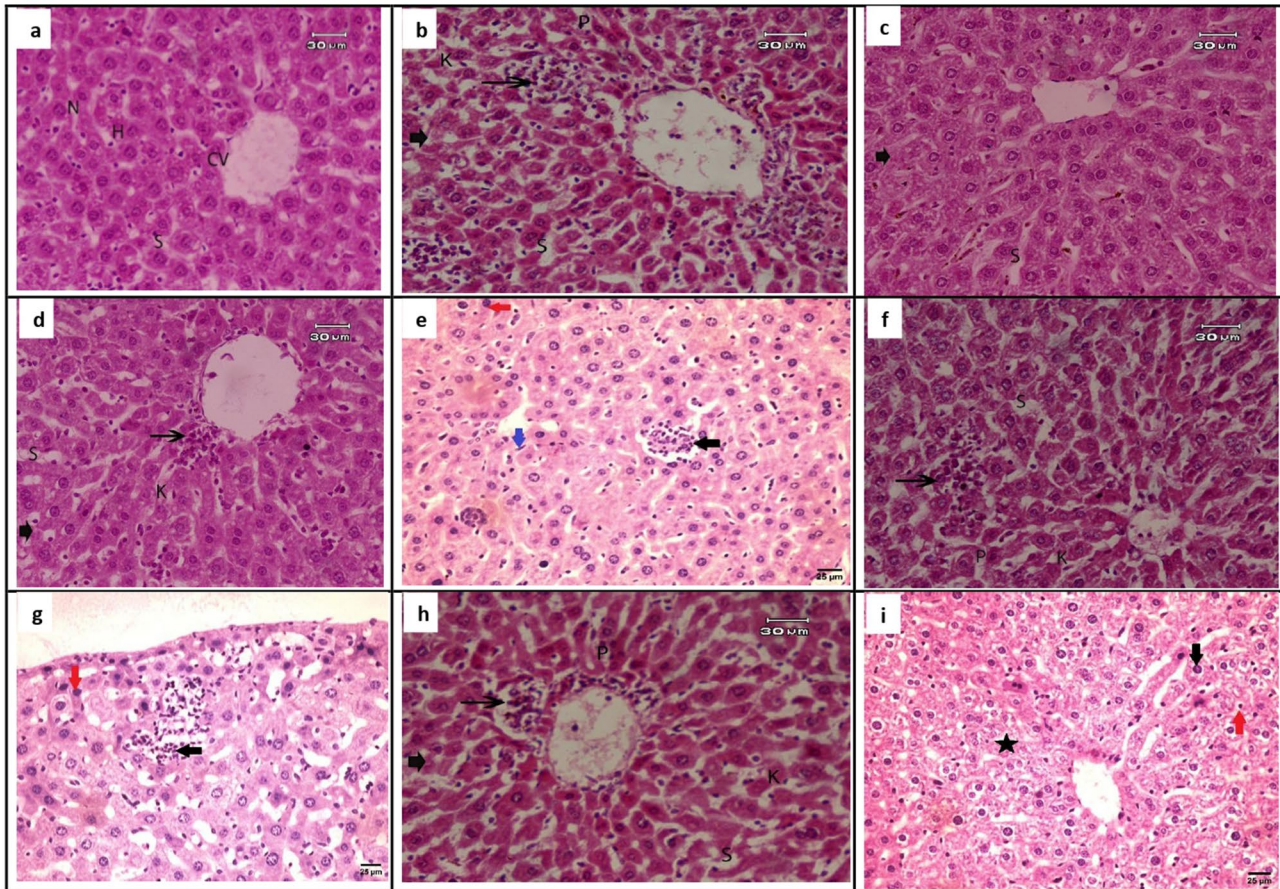


**Fig. 6** Liver sections of different study groups (Hematoxylin and Eosin, Scale bar 25–30  $\mu$ m, X400). **a** GI showing hepatic architecture. The central vein (CV), hepatocytes (H), blood sinusoids (S) and nucleus (S) were noticed. **b** GII showing degeneration changes with eosinophilic cytoplasm necrotic areas (arrowhead) associated with focal mononuclear cell infiltration (arrow), and dilated sinusoidal (S), deeply pyknotic nuclei (P) with mild activation of Kupffer cells (K). **c** GIII showing ameliorative effect with few degeneration (arrowhead), enlargement of sinusoids (S), minimum activation of Kupffer cells (K). **d** GIV showing ameliorative effect with few inflammatory cells around central vein (arrow), enlargement of sinusoids (S), minimum activation of Kupffer cells (K). **e** GV showing focal infiltration of mononuclear inflammatory cells between hepatocytes (black arrow) with activation of van kupffer cells (blue arrow) and some hepatocytes showing pyknotic nuclei (red arrow). **f** GVI showing degeneration, mild necrosis (arrowhead), inflammatory cell infiltration (arrow), enlargement of sinusoids (S), mild activation of Kupffer cells (K) and pyknotic nuclei (P). **g** GVII showing focal infiltration of mononuclear inflammatory cells between hepatocytes (black arrow) and some hepatocytes showing pyknotic nuclei (red arrow). **h** GVIII showing degeneration, mild necrosis (arrowhead), inflammatory cell infiltration around central vein (arrow), enlargement of sinusoids (S), mild activation of Kupffer cells (K) and pyknotic nuclei (P). **i** GIX showing necrobiotic changes in some hepatocytes (star), presence of pyknotic nuclei in others (black arrow) and presence of few numbers of mononuclear inflammatory cells in hepatic sinusoids (red arrow).

[GI (normal control), GII (infected control), GIII (infected, NPs treated), GIV (infected, BV treated), GV (infected, BVL-MOFs-NPs), GVI (infected, spiramycin treated), GVII (infected, SL-MOFs-NPs), GVIII (infected, ciprofloxacin treated), GIX (infected, CL-MOFs-NPs)]

and presence of few numbers of mononuclear inflammatory cells in hepatic sinusoids (Fig. 6i).

### Kidney

Examination of kidney sections from GI showed normal structure of the glomeruli, urinary spaces and Bowman's capsules. Renal tubules (proximal convoluted and distal convoluted tubules) exhibit normal structure (Fig. 7a), from GII showed hydropic degeneration, necrosis and

pyknotic nuclei were observed significantly in tubules epithelial cells. Focal inflammatory cells were seen in the intertubular areas and around glomerulus. Bowman capsule of glomerulus were observed to be enlarged whereas some parts of it was found to be narrow (Fig. 7b), from GIII, GIV showed ameliorative effect with degeneration, necrosis and pyknotic nuclei, focal inflammatory cells were seen in the intertubular areas (Fig. 7c, d), from GV showed focal infiltration by mononuclear inflammatory cells between renal tubules with hypotrophy in some

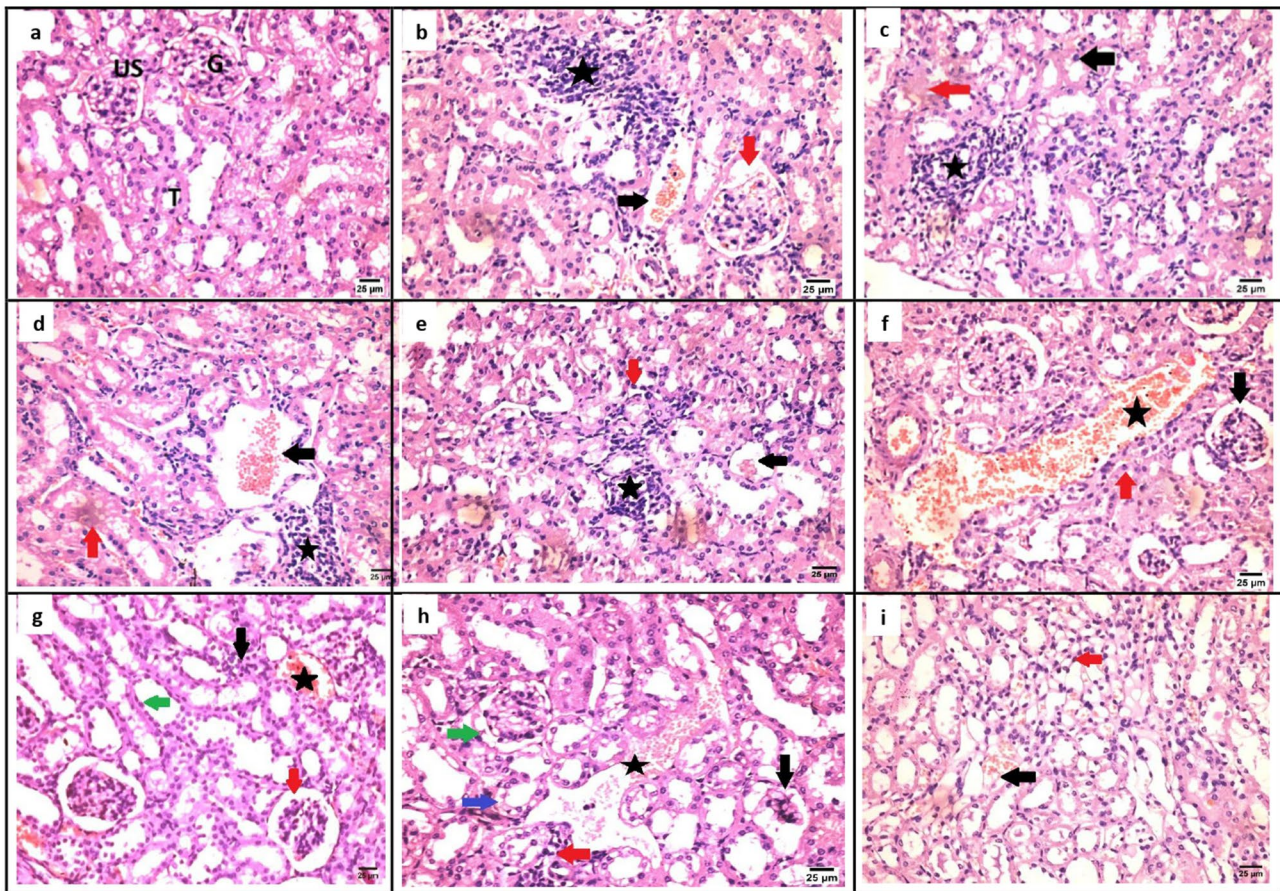


**Fig. 7** Kidney sections of different study groups (Hematoxylin and Eosin, Scale bar 25  $\mu$ m, X400). **a** GI showing normal structure of kidney including glomerulus (G), urinary space, (US) tubules (T). **b** GII showing focal infiltration by mononuclear inflammatory cells between renal tubules (star) with congestion of peritubular blood vessels (black arrow) and widening urinary space (red arrow). **c** GIII showing focal infiltration by mononuclear inflammatory cells between renal tubules (star), some renaltubules showing necrobiotic changes (red arrow) and presence of pyknotic nuclei in renal tubular epithelium (black arrow). **d** GIV showing focal infiltration by mononuclear inflammatory cells between renal tubules (star) with congestion of peritubular blood vessels (black arrow) and some renaltubules showing necrobiotic changes (red arrow). **e** GV showing focal infiltration by mononuclear inflammatory cells between renal tubules (star) with hypotrophy in some glomeruli (black arrow) and presence of pyknotic nuclei in renal tubular epithelium (black arrow). **f** GVI showing degeneration (arrowhead), pyknotic nuclei (P) were

glomeruli and presence of pyknotic nuclei in renal tubular epithelium (Fig. 7e), from GVI, GVIII showed necrosis and pyknotic nuclei were observed significantly in tubules epithelial cells. Atrophy of glomerulus and winding urinary space was also observed (Fig. 7f, h) from GVII showed focal infiltration by mononuclear inflammatory cells between renal tubules with congestion of peritubular blood vessels, widening urinary space and presence of pyknotic nuclei in renal tubular epithelium (Fig. 7g), from

observed in tubules epithelial cells. **g** GVII showing focal infiltration by mononuclear inflammatory cells between renal tubules (black arrow) with congestion of peritubular blood vessels (star), widening urinary space (red arrow) and presence of pyknotic nuclei in renal tubular epithelium (green arrow). **h** GVIII showing hypotrophy (black arrow) and others showing widening urinary space (green arrow), some renal tubules showing degenerative changes (blue arrow), presence of focal infiltration by mononuclear inflammatory cells between renal tubules (red arrow) with congestion of peritubular blood vessels (star). **i** GIX showing disorganization (D) showing congestion of peritubular blood vessels (black arrow) and presence of pyknotic nuclei in renal tubular epithelium (red arrow). [GI (normal control), GII (infected control), GIII (infected, NPs treated), GIV (infected, BV treated), GV (infected, BVL-MOFs-NPs), GVI (infected, spiramycin treated), GVII (infected, SL-MOFs-NPs), GVIII (infected, ciprofloxacin treated), GIX (infected, CL-MOFs-NPs)]

GIX showed congestion of peritubular blood vessels and presence of pyknotic nuclei in renal tubular epithelium (Fig. 7i).

### Immunohistochemical results

Liver sections from GII showed high density CD8<sup>+</sup> infiltration, from GIII, GVI, GVII, GVIII, and GIX showed low

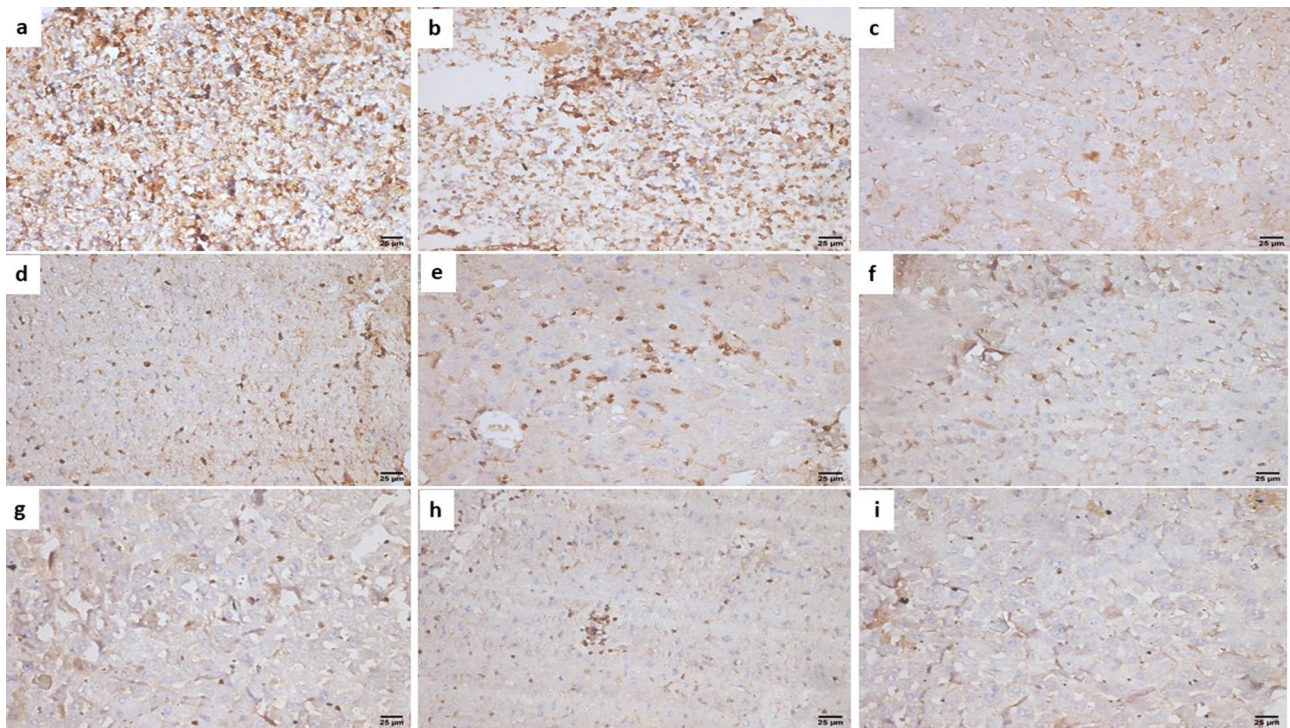


**Fig. 8** IHC results for liver sections of different study groups (IHC-peroxidase-DAB, X400). **a, b** GII showing high expression of CD8<sup>+</sup>. **c** GIII showing low expression of CD8<sup>+</sup>. **d** GIV showing intermediate expression of CD8<sup>+</sup>. **e** GV showing intermediate expression of CD8<sup>+</sup>. **f** GVI showing low expression of CD8<sup>+</sup>. **g** GVII showing low expression of CD8<sup>+</sup>. **h** GVIII showing low expression of CD8<sup>+</sup>.

**i** GIX showing low expression of CD8<sup>+</sup>. [GI (normal control), GII (infected control), GIII (infected, NPs treated), GIV (infected, BV treated), GV (infected, BVL-MOFs-NPs), GVI (infected, spiramycin treated), GVII (infected, SL-MOFs-NPs), GVIII (infected, ciprofloxacin treated), GIX (infected, CL-MOFs-NPs)]

density CD8<sup>+</sup> infiltration while from GIV, and GV showed intermediate density CD8<sup>+</sup> infiltration (Fig. 8).

## Discussion

Al-BDC MOFs has been used to create MOF capsulated BV composites (BVL-MOFs-NPs), the crystalline phase of Al-BDC MOFs and BV incorporated into MOF–matrix showed highly crystalline phase with good diffraction and this results are agree with previous reported work (Gordon et al. 2015). The surface of prepared material and incorporated with BV are essential requirement to use these MOFs as drug delivery systems, it showed well-distributed and homogeneous with the morphology of hexagonal bipyramidal structure, this results was agreement with previous work (Nguyen et al. 2019).

In the present study, the therapeutic effect of BV and BVL-MOFs-NPs were evaluated for the treatment of murine chronic toxoplasmosis and the results were compared with spiramycin and ciprofloxacin also alone and after loading on MOFs-NPs. The most common used therapeutic medicines for *T. gondii* infection are pyrimethamine and

sulfadiazine. For patients with hypersensitivity to sulfonamides, pyrimethamine alone in high dosages or in combination with clindamycin, clarithromycin, azithromycin or atovaquone can be used as substitutes (Wei et al. 2015). The usual pyrimethamine-based therapy is accompanied with side effects and other restrictions as Pyrimethamine acts on the folate biosynthesis pathway, inhibiting dihydrofolate reductase activity and thus eventually blocking nucleic acid synthesis (Elsheikha et al. 2020). Notably, treating asymptomatic toxoplasmosis and infection in pregnant females, spiramycin that have minimal foetal toxicity with rapid killing of tachyzoites and azithromycin are the most widely used drugs but unfortunately, spiramycin has low bioavailability and poor penetration of the blood brain barrier (Wei et al. 2015). Furthermore, spiramycin loaded chitosan NPs was proved to reduce the mortality rate, reduce the parasite number, and improve the histopathological picture of brain, eye, liver, and spleen in the infected treated groups compared to the infected controls (Eteawa et al. 2018). Moreover, ciprofloxacin and other nitrofurans derived quinolones are effective antibacterial, anti-mycoplasma, and antiprotozoal agents that act through inhibition of DNA replication. They were proved to be effective against acute toxoplasmosis

with depression of intracellular proliferation and their efficacy was enhanced by loading on silver NPs (Ahmed et al. 2022; Sadeghi et al. 2022). Regrettably, ciprofloxacin can hinder the fetus's ability to synthesize DNA, leading to both organ mutagenesis and agenesis (Yefet et al. 2018). Furthermore, BV was successfully tried as an antiparasitic drug against *Trypanosoma brucei brucei* (Boulanger et al. 2002; Boutrin et al. 2008), *Entamoeba histolytica* (SABER et al. 2017), *Plasmodium falciparum* (Deregnaucourt and Schrével 2000), *Plasmodium berghei* (Moreira et al. 2002). However, all the available therapies against *Toxoplasma* can only affect tachyzoites with no or poor effect against chronic tissue cysts (Montazeri et al. 2017; Tiwari et al. 2019).

In the present study, BV was administered through subcutaneous injection and its therapeutic effect on chronically infected mice with *Toxoplasma* was tested alone and after loading on MOFs-NPs. Kim et al. reported no significant adverse reactions affecting the CNS, CVS, GIT, and the respiratory system as a result of BV injection through subcutaneous route (Kim et al. 2004). Besides, Carpena et al. reported that it is difficult to give BV orally as it is easily digested by gastrointestinal enzymes which will greatly reduce its biological efficacy (Carpena et al. 2020). BV is characterized by a relatively short half-life in plasma that makes it difficult to estimate the proper dose of BV. Researchers and authors tried to overcome that problem by developing combinations between BV and other polymers and NPs (Xing et al. 2003).

In the present study, parasitological examination by counting brain cyst count was done. This agreed with Grande et al. who proved a strong predilection of *Toxoplasma* parasite to the brain tissue with formation of intracellular cysts in the neurons and the glial tissue (Del Grande et al. 2017). Counting of *Toxoplasma* brain cysts in different study groups showed high statistically significant difference ( $P < 0.001$ ) between the different infected treated groups and the infected control (GII). GV (infected, treated with BVL-MOFs-NPs) showed the least count of brain cysts; mean  $\pm$  SD ( $281 \pm 29.5$ ) with highest percentage of reduction of brain cyst count (53.6%) although there was no statistically significant difference with the other infected treated groups. This is alongside with Mohammad et al. study in which a statistically significant difference ( $P < 0.001$ ) was recorded between the study groups and the positive control group. The lowest brain cyst count was recorded in animal groups treated with *Nigella sativa* oil loaded on Copper-benzene tricarboxylic acid metal organic frame works (NSO@Cu-BTC MOF) followed by the group treated by a combination of wheat germ and *Nigella sativa* oils that were loaded on Cu-BTC MOF (WGO + NSO@Cu-BTC MOF) then WGO@Cu-BTC MOF, with a considerable reduction of the brain cyst burden (64.3, 51.4 and 49.5% respectively). They also recorded moderate percentages of reduction of brain cyst count in the groups

treated with spiramycin alone and spiramycin@Cu-BTC MOF (42.4%, 41.8%, respectively) which is similar to a great extent with this study as the groups treated with spiramycin alone and SL-MOF NPs showed percentages of reduction (48.5%, 49.6%, respectively) This study used the same time schedule for starting drug administration at 8 wpi and animal sacrifice at 10 wpi. They also used the same *ME49* strain of *Toxoplasma* for animal infection but unlike our study they used spiramycin alone and loaded on Cu-BTC MOF in a dose of 200 mg/kg body weight/day which is double the dose used in this study which may explain its poor results compared with the above mentioned treated groups (Mohammad et al. 2023). These results are comparable with Etewa et al. who reported a significant reduction ( $P < 0.001$ ) in the size and number of *Toxoplasma* brain cysts in the groups of mice treated with spiramycin-pyrimethamine-folinic acid (SPF) combination and to less extent the group treated with bone marrow derived mesenchymal stem cells combined with SPF compared to the chronically infected control group. They used the same dose of spiramycin as in this study (100 mg/kg/day) but started 6 wpi only for 10 days (Etewa et al. 2019). This concurs with a study that revealed a significant reduction ( $P < 0.001$ ) in the mean number of *Toxoplasma* cysts in the brain and liver tissues in the infected groups treated either by spiramycin alone or spiramycin loaded chitosan NPs compared to infected control mice. Worthwhile, the authors used spiramycin alone and spiramycin loaded chitosan NPs in a dose of (100 mg/kg/day) started 6 wpi for 10 days (Etewa et al. 2018). These results are also in congruence with El-Ashkar et al. who recorded a significant reduction in the brain cyst count in the spiramycin-metronidazole treated group compared to infected control. In such study, spiramycin was used in a dose of 400 mg/kg and metronidazole dose was 500 mg/kg. The drugs were given orally as liquid suspensions, by gavage, daily for 7 days; starting 8 wpi (El-Ashkar et al. 2020). This study recorded that the lowest percentage of reduction of brain cyst count (22.8%) in the group treated with MOF-NPs which could be concluded as MOF-NPs has a weak therapeutic effect when used alone. This result is in congruence with Mohammad et al. study in which lowest percentage of reduction of brain cyst count (24.4%) in the group treated with Cu-BTC MOF (Mohammad et al. 2023). This also agrees with a study that revealed the lowest therapeutic effect of Cu-BTC when used alone (Soltani and Akhbari 2022).

In the present study, histopathological examination of tissue sections from brain, eye, liver, and kidney of chronically infected mice with *Toxoplasma* showed a marked ameliorative effect of BV administration when used alone or loaded on MOFs-NPs. It significantly reduced tissue inflammation, degeneration, and fibrosis. This concurs with studies that reported significant therapeutic effects of BV. Park et al. reported a significant hepatoprotective effect of

BV through suppression of antiapoptotic effects of tumor necrosis factor-alpha and actinomycin D (Park et al. 2010). Han et al. highlighted the potential role of BV on promoting cell regeneration with subsequent wound healing (Han et al. 2013). BV was successfully used in patients with rheumatoid arthritis and other autoimmune diseases as it has an important immunomodulatory effects that greatly improved the clinical manifestations of these diseases (Son et al. 2007; Khalil et al. 2021). BV has an important antimicrobial activity against both gram-positive and gram-negative bacteria and some fungi especially belong to *Candida* species. The antimicrobial properties of BV were mainly due to melittin and PLA2 components (Al-Ani et al. 2015; Abd El-Wahed et al. 2018). Regarding application of BV in controlling parasitic diseases, BV PLA2 was reported to have a significant role in inhibiting oocyst development of *Plasmodium berghei* in the gut of *Anopheles stephensi* mosquito (Moreira et al. 2002). It is worth mentioning that BV was successfully inhibit the development of intraerythrocytic stages of *Plasmodium falciparum* (Deregnacourt and Schrével 2000). Besides, BV PLA2 was found to have a lethal effect on *Trypanosoma brucei brucei* (Boulanger et al. 2002; Boutrin et al. 2008). Moreover, BV was proven successfully to have a lethal effect on *S. mansoni* eggs and miracidia (Boutrin et al. 2008). Furthermore, BV was reported to have an important amoebicidal activity against *Entamoeba histolytica* (SABER et al. 2017).

In the present study, MOFs-NPs significantly enhanced the therapeutic effect of BV against murine toxoplasmosis. This concurs with Mohammad et al. who revealed outstanding results when Cu-BTC MOF was used with NSO, WGO, and combination of both oils in *Toxoplasma* infected mice (Mohammad et al. 2023). This also agrees with Saber et al. who proved that BVL-MOFs-NPs amoebicidal effect was greater than BV alone (SABER et al. 2017). Also, Al-Hatamleh et al. reported enhancement of the bee products therapeutic effects by alginate-based nanomaterials (Al-Hatamleh et al. 2022). This is in congruence with Tawfeek et al. who reported enhancement of antischistosomal activity of praziquantel in *S. mansoni* infected mice when loaded on silica NPs (Tawfeek et al. 2019).

In the present study, IHC examination of liver tissue revealed high density CD8<sup>+</sup> infiltration in GII (infected control). This is in congruence with studies that reported high density CD8<sup>+</sup> infiltration around *Toxoplasma* brain cyst (Schlüter et al. 1997; Bhadra et al. 2011; Eteawa et al. 2019). Literature proved the important role of CD8 + T-cells in controlling *Toxoplasma* tissue cysts (Scharton-Kersten et al. 1996; Bhadra et al. 2011). Suzuki et al. reported a significant role of CD8 + T-cells in eradicating *Toxoplasma* brain cyst in BALB/C mice through perforin mediated effector pathway (Suzuki et al. 2010). Liver sections from GIII (infected, MOFs-NPs treated),

GVI (infected, spiramycin treated), GVII (infected, SL-MOFs-NPs treated), GVIII (infected, ciprofloxacin treated), GIX (infected, CL-MOFs-NPs treated) showed low density CD8<sup>+</sup> infiltration while, intermediate density CD8<sup>+</sup> infiltration was noted in liver sections from GIV (infected, BV treated), and GV (infected, BVL-MOFs-NPs treated). This also concurs with Eteawa et al. who reported low density CD8<sup>+</sup> infiltration in the infected mice treated with spiramycin-pyrimethamine-folinic acid combination (Eteawa et al. 2019). Our results are also comparable to Kamiński et al. who reported an immunosuppressive role of ciprofloxacin on human T-cells through inhibition of IL-2 and IL-4 expression (Kamiński et al. 2010). Our results also agree with the studies performed on BV and reported their important role in the treatment of rheumatoid arthritis, psoriasis, and other autoimmune diseases due to its immunosuppressive, and immunomodulating activities by decrease serum levels of IL-2 and IL-12 that are important for T-cell activation, and increase serum level of the inhibitory IL-10 (Son et al. 2007; Ahmed et al. 2017).

## Conclusion and recommendation

BVL-MOFs-NPs is a promising therapy against chronic toxoplasmosis. It could effectively reduce the number of tissue cysts although there was no statistically significant difference with the other infected treated groups. Also, it was recorded to ameliorate tissue inflammation, degeneration, and fibrosis in liver, kidney, eye, and brain tissues with moderate immunomodulation in the affected tissues as reported by the histopathological and IHC studies. Further lab studies should be done to assess the possible adverse reactions of using BV before start of clinical trials on human.

**Acknowledgements** We would like to acknowledge the administration of NRC for their help and support throughout the experiment.

**Author contribution** HME, MMA, and AEK designed the plan of work and performed the parasitological examination, RMA performed the immunohistochemical examination of hepatic sections, AMB, and SASS supervised animal housing, *Toxoplasma* strain maintenance, animal drug administration, and animal sacrifice. EAM, shared in designing the plan of work, analysing the data, writing, and revising the manuscript. The manuscript has been read and approved by all named authors. We further confirm that the order of authors listed has been approved by all of us.

**Funding** There has been no financial support for this work that could have influenced its outcome.

## Declarations

**Conflicts of interest** None.

## References

- Abd El-Wahed A, Khalifa S, Sheikh B, et al (2018) Bee venom composition: from chemistry to biological activity. In: Studies in natural products chemistry. Elsevier BV, pp 459–484
- Abdelhameed R, Abdel-Gawad H, Elshahat M, Emam H (2016) Cu–BTC@cotton composite: design and removal of ethion insecticide from water. *RSC Adv* 6:42324–42333
- Acar S, Keskin-Arslan E, Erol-Coskun H et al (2019) Pregnancy outcomes following quinolone and fluoroquinolone exposure during pregnancy: a systematic review and meta-analysis. *Reprod Toxicol* 85:65–74. <https://doi.org/10.1016/J.REPROTOX.2019.02.002>
- Adade C, Oliveira I, Pais J, Souto-Padrón T (2013) Melittin peptide kills *Trypanosoma cruzi* parasites by inducing different cell death pathways. *Toxicol* 69:227–239. <https://doi.org/10.1016/J.TOXICON.2013.03.011>
- Ahmed O, Fahim H, Mahmoud A, Ahmed E (2017) Bee venom and hesperidin effectively mitigate complete Freund's adjuvant-induced arthritis via immunomodulation and enhancement of antioxidant defense system. *Arch Rheumatol* 33:198–212. <https://doi.org/10.5606/ARCHRHEUMATOL.2018.6519>
- Ahmed F, Rashed S, Abououf E, et al (2022) Effects of Ciprofloxacin loaded on silver nanoparticles on murine acute toxoplasmosis. *Benha Med J* <https://doi.org/10.21608/bmfj.2022.116115.1529>
- Alajmi R, AL-Megrin W, Metwally D, et al (2019) Anti-toxoplasma activity of silver nanoparticles green synthesized with phoenix dactylifera and ziziphus spina-christi extracts which inhibits inflammation through liver regulation of cytokines in Balb/c mice. *Biosci Rep*. <https://doi.org/10.1042/BSR20190379>
- Al-Ani I, Zimmermann S, Reichling J, Wink M (2015) Pharmacological synergism of bee venom and melittin with antibiotics and plant secondary metabolites against multi-drug resistant microbial pathogens. *Phytomedicine* 22:245–255. <https://doi.org/10.1016/J.PHYMED.2014.11.019>
- Al-Hatamleh M, Alshar W, Hatmal M et al (2022) Applications of alginate-based nanomaterials in enhancing the therapeutic effects of bee products. *Front Mol Biosci*. <https://doi.org/10.3389/FMOLB.2022.865833>
- Baek H, Jang H, Jeon H, Bae H (2018) Comparison of administration routes on the protective effects of Bee Venom Phospholipase A2 in a mouse model of Parkinson's disease. *Front Aging Neurosci* 10:1–8. <https://doi.org/10.3389/fnagi.2018.00179>
- Bhadra R, Gigley J, Weiss L, Khan I (2011) Control of *Toxoplasma* reactivation by rescue of dysfunctional CD8+ T-cell response via PD-1-PDL-1 blockade. *Proc Natl Acad Sci U S A* 108:9196–9201. <https://doi.org/10.1073/PNAS.1015298108>
- Boivin G, Bottomley M, Grobe N (2016) Responses of male C57BL/6N mice to observing the euthanasia of other mice. *J Am Assoc Lab Anim Sci* 55:406–411
- Boulanger N, Brun R, Ehret-Sabatier L et al (2002) Immunopeptides in the defense reactions of *Glossina morsitans* to bacterial and *Trypanosoma brucei* infections. *Insect Biochem Mol Biol* 32:369–375. [https://doi.org/10.1016/S0965-1748\(02\)00029-2](https://doi.org/10.1016/S0965-1748(02)00029-2)
- Boutrin M, Foster H, Pentreath V (2008) The effects of bee (*Apis mellifera*) venom phospholipase A2 on *Trypanosoma brucei* and enterobacteria. *Exp Parasitol* 119:246–251. <https://doi.org/10.1016/J.EXPPARA.2008.02.002>
- Carpena M, Nuñez-Estevez B, Soria-Lopez A, Simal-Gandara J (2020) Bee venom: an updating review of its bioactive molecules and its health applications. *Nutrients* 12:1–27. <https://doi.org/10.3390/NU12113360>
- CDC (2020) Parasites – Toxoplasmosis
- Chew W, Segarra I, Ambu S, Mak J (2012) Significant reduction of brain cysts caused by *Toxoplasma gondii* after treatment with spiramycin coadministered with metronidazole in a mouse model of chronic toxoplasmosis. *Antimicrob Agents Chemother* 56:1762–1768. <https://doi.org/10.1128/AAC.05183-11>
- Del Grande C, Galli L, Schiavi E et al (2017) Is *Toxoplasma gondii* a Trigger of Bipolar Disorder? *Pathogens*. <https://doi.org/10.3390/PATHOGENS6010003>
- Deregnacourt C, Schrével J (2000) Bee venom phospholipase A2 induces stage-specific growth arrest of the intraerythrocytic *Plasmodium falciparum* via modifications of human serum components. *J Biol Chem* 275:39973–39980. <https://doi.org/10.1074/JBC.M006712200>
- Djurkovic-Djakovic O, Milenković V, Nikolić A et al (2002) Efficacy of atovaquone combined with clindamycin against murine infection with a cystogenic (Me49) strain of *Toxoplasma gondii*. *J Antimicrob Chemother* 50:981–987. <https://doi.org/10.1093/JAC/DKF251>
- El Fakhry Y, Achbarou A, Desportes-Livage I, Mazier D (1998) Encephalitozoon intestinalis: humoral responses in interferon- $\gamma$  receptor knockout mice infected with a microsporidium pathogenic in AIDS patients. *Exp Parasitol* 89:113–121. <https://doi.org/10.1006/expr.1998.4267>
- EL-Ashkar A, El-Hosseiny L, AbuZahra F, et al (2020) Potential therapeutic effect of allogenic mesenchymal stem cells on chronic cerebral murine toxoplasmosis. *Afro-Egyptian J Infect Endem Dis* <https://doi.org/10.21608/aeji.2020.23818.1051>
- El-Shafey A, Hegab M, Seliem M et al (2020) Curcumin@metal organic frameworks nano-composite for treatment of chronic toxoplasmosis. *J Mater Sci Mater Med*. <https://doi.org/10.1007/S10856-020-06429-Y>
- Elsheikha H, Marra C, Zhu X (2020) Epidemiology, pathophysiology, diagnosis, and management of cerebral toxoplasmosis. *Clin Microbiol Rev* 34:1–28. <https://doi.org/10.1128/CMR.00115-19>
- Emam H, Ahmed H, El-Deib H et al (2019) Non-invasive route for desulfurization of fuel using infrared-assisted MIL-53(Al)-NH2 containing fabric. *J Colloid Interface Sci* 556:193–205. <https://doi.org/10.1016/J.JCIS.2019.08.051>
- Etewa S, El-Maaty D, Hamza R et al (2018) Assessment of spiramycin-loaded chitosan nanoparticles treatment on acute and chronic toxoplasmosis in mice. *J Parasit Dis* 42:102–113. <https://doi.org/10.1007/S12639-017-0973-8>
- Etewa S, Al-Hoot A, Abdelmoaty S, et al (2019) The outcomes of mesenchymal stem cells therapy for experimental toxoplasmosis. *Parasitol United J* <https://doi.org/10.21608/puj.2019.7541.1030>
- Feldman AT, Wolfe D (2014) Tissue processing and hematoxylin and eosin staining. *Methods Mol Biol* 1180:31–43. [https://doi.org/10.1007/978-1-4939-1050-2\\_3](https://doi.org/10.1007/978-1-4939-1050-2_3)
- Garcia L, Bruckner D (1997) Diagnostic medical parasitology. 3rd ed. ASM Press, Washington DC
- Gherbawy Y, Shalaby I, El-Sadek M et al (2013) The anti-fascioliasis properties of silver nanoparticles produced by *Trichoderma harzianum* and their improvement of the anti-fascioliasis drug Triclabendazole. *Int J Mol Sci* 14:21887–21898. <https://doi.org/10.3390/ijms141121887>
- Gordon J, Kazemian H, Rohani S (2015) MIL-53(Fe), MIL-101, and SBA-15 porous materials: potential platforms for drug delivery. *Mater Sci Eng C Mater Biol Appl* 47:172–179. <https://doi.org/10.1016/J.MSEC.2014.11.046>
- Hagras N, Allam A, Farag H et al (2019) Successful treatment of acute experimental toxoplasmosis by spiramycin-loaded chitosan nanoparticles. *Exp Parasitol*. <https://doi.org/10.1016/J.EXPPARA.2019.107717>
- Hamidović A, Etougébéché J, Tonouhewa A et al (2021) A hotspot of *Toxoplasma gondii* Africa I lineage in Benin: How new genotypes from West Africa contribute to understand the parasite genetic diversity worldwide. *PLoS Negl Trop Dis* 15:1–16. <https://doi.org/10.1371/JOURNAL.PNTD.0008980>

- Han S, Park K, Nicholls Y et al (2013) Effects of honeybee (*Apis mellifera*) venom on keratinocyte migration in vitro. *Pharmacogn Mag* 9:220–226. <https://doi.org/10.4103/0973-1296.113271>
- Hegazi A, Abdou A, El-Moez S, Allah F (2014) Evaluation of the antibacterial activity of bee venom from different sources. *World Appl Sci Journal* 30:266–270
- Jakob T, Rafei-Shamsabadi D, Spillner E, Müller S (2017) Diagnostics in Hymenoptera venom allergy: current concepts and developments with special focus on molecular allergy diagnostics. *Allergo J* 26:33–48. <https://doi.org/10.1007/s40629-017-0014-2>
- Kamiński M, Sauer S, Klemke C et al (2010) Mitochondrial reactive oxygen species control T cell activation by regulating IL-2 and IL-4 expression: mechanism of ciprofloxacin-mediated immunosuppression. *J Immunol* 184:4827–4841. <https://doi.org/10.4049/JIMMUNOL.0901662>
- Khalil A, Elesawy B, Ali T, Ahmed O (2021) Bee venom: From venom to drug. *Molecules* 26:1–17. <https://doi.org/10.3390/molecules26164941>
- Khan I, Saeed K, Khan I (2019) Nanoparticles: properties, applications and toxicities. *Arab J Chem* 12:908–931. <https://doi.org/10.1016/J.ARABJC.2017.05.011>
- Kim H, Kwon Y, Ham T et al (2004) General pharmacological profiles of bee venom and its water soluble fractions in rodent models. *J Vet Sci* 5:309–3018
- Lachkhem A, Galal L, Lahmar I et al (2021) First isolation and genotyping of *Toxoplasma gondii* strains from domestic animals in Tunisia. *Sci Rep*. <https://doi.org/10.1038/S41598-021-88751-1>
- Lee K, Kim B, Yoon H et al (2016) Secapin, a bee venom peptide, exhibits anti-fibrinolytic, anti-elastolytic, and anti-microbial activities. *Dev Comp Immunol* 63:27–35. <https://doi.org/10.1016/J.DCI.2016.05.011>
- Martins-Duarte E, Dubar F, Lawton P et al (2015) Ciprofloxacin derivatives affect parasite cell division and increase the survival of mice infected with *Toxoplasma gondii*. *PLoS One*. <https://doi.org/10.1371/JOURNAL.PONE.0125705>
- Matta S, Rinkenberger N, Dunay I, Sibley L (2021) *Toxoplasma gondii* infection and its implications within the central nervous system. *Nat Rev Microbiol* 19:467–480. <https://doi.org/10.1038/S41579-021-00518-7>
- McKinlay A, Morris R, Horcajada P et al (2010) BioMOFs: metal-organic frameworks for biological and medical applications. *Angew Chem Int Ed Engl* 49:6260–6266. <https://doi.org/10.1002/ANIE.201000048>
- Mohammad O, El Naggar H, Abdelmaksoud H et al (2023) The effect of *Nigella sativa* oil- and wheat germ oil-loaded metal organic frameworks on chronic murine toxoplasmosis. *Acta Trop*. <https://doi.org/10.1016/J.ACTATROPICA.2023.106823>
- Montazeri M, Rezaei K, Ebrahimzadeh M et al (2017) Survey on synergism effect of ketotifen in combination with pyrimethamine in treatment of acute murine toxoplasmosis. *Trop Med Health*. <https://doi.org/10.1186/S41182-017-0079-0>
- Moreira L, Ito J, Ghosh A et al (2002) Bee venom phospholipase inhibits malaria parasite development in transgenic mosquitoes. *J Biol Chem* 277:40839–40843. <https://doi.org/10.1074/JBC.M206647200>
- Nguyen T, Ninh H, Tran C et al (2019) Size-control and surface modification of flexible metal-organic framework MIL-53 (Fe) by polyethyleneglycol for 5-fluorouracil anticancer drug delivery. *ChemistrySelect* 4:2333–2338
- Omidian M, Asgari Q, Bahreini M et al (2022) Acute toxoplasmosis can increase serum dopamine level. *J Parasit Dis* 46:337–342. <https://doi.org/10.1007/S12639-021-01447-1>
- Park J, Kim K, Kim S et al (2010) Bee venom protects hepatocytes from tumor necrosis factor-alpha and actinomycin D. *Arch Pharm Res* 33:215–223. <https://doi.org/10.1007/S12272-010-0205-6>
- Pucca M, Ahmadi S, Cerni F et al (2020) Unity makes strength: exploring intraspecies and interspecies toxin synergism between phospholipases A2 and cytotoxins. *Front Pharmacol*. <https://doi.org/10.3389/FPHAR.2020.00611>
- Quijia C, Alves R, Hanck-Silva G et al (2022) Metal-organic frameworks for diagnosis and therapy of infectious diseases. *Crit Rev Microbiol* 48:161–196. <https://doi.org/10.1080/1040841X.2021.1950120>
- Rayani M, Unyah N, Vafafar A, Hatam G (2020) Isoenzyme profiles and phylogenetic analysis of *Giardia duodenalis* isolates from Iranian patients. *Environ Sci Pollut Res* 27:40652–40663. <https://doi.org/10.1007/s11356-020-10062-1>
- Saber A, Abdelwahab A, el Amir A et al (2017) BEE venom loaded chitosan nanoparticles as treatment for Amoebiasis in mice. *J Egypt Soc Parasitol* 47:443–458
- Sadeghi M, Sarvi S, Emami S et al (2022) Evaluation of anti-parasitic activities of new quinolones containing nitrofurans moiety against *Toxoplasma gondii*. *Exp Parasitol*. <https://doi.org/10.1016/J.EXPPARA.2022.108344>
- Saleh A, Badr A, Mahmoud S et al (2020) In-vitro investigation of the effect of bee venom on *Schistosoma mansoni* eggs. *Int J Vet Sci* 9:473–475
- Scharton-Kersten T, Wynn T, Denkers E et al (1996) In the absence of endogenous IFN-gamma, mice develop unimpaired IL-12 responses to *Toxoplasma gondii* while failing to control acute infection. *J Immunol* 157:4045–4054
- Schlüter D, Kaefer N, Hof H et al (1997) Expression pattern and cellular origin of cytokines in the normal and *Toxoplasma gondii*-infected murine brain. *Am J Pathol* 150:1021–1035
- Shammaa A, Powell T, Benmerzouga I (2021) Adverse outcomes associated with the treatment of *Toxoplasma* infections. *Sci Rep*. <https://doi.org/10.1038/S41598-020-80569-7>
- Shin W, Cho J, Kannan A et al (2016) Cross-linked composite gel polymer electrolyte using mesoporous methacrylate-functionalized SiO<sub>2</sub> nanoparticles for lithium-ion polymer batteries. *Sci Rep* 6:1–10. <https://doi.org/10.1038/srep26332>
- Soltani S, Akhbari K (2022) Cu-BTC metal-organic framework as a biocompatible nanoporous carrier for chlorhexidine antibacterial agent. *J Biol Inorg Chem* 27:81–87. <https://doi.org/10.1007/S00775-021-01912-5>
- Son D, Lee J, Lee Y et al (2007) Therapeutic application of anti-arthritis, pain-releasing, and anti-cancer effects of bee venom and its constituent compounds. *Pharmacol Ther* 115:246–270. <https://doi.org/10.1016/J.PHARMTHERA.2007.04.004>
- Sun C, Qin C, Wang X, Su Z (2013) Metal-organic frameworks as potential drug delivery systems. *Expert Opin Drug Deliv* 10:89–101. <https://doi.org/10.1517/17425247.2013.741583>
- Suzuki Y, Wang X, Jortner B et al (2010) Removal of *Toxoplasma gondii* cysts from the brain by perforin-mediated activity of CD8+ T cells. *Am J Pathol* 176:1607–1613. <https://doi.org/10.2353/AJPATH.2010.090825>
- Tawfeek G, Baki M, Ibrahim A et al (2019) Enhancement of the therapeutic efficacy of praziquantel in murine Schistosomiasis mansoni using silica nanocarrier. *Parasitol Res* 118:3519–3533. <https://doi.org/10.1007/S00436-019-06475-8>
- Tiwari A, Hannah R, Lutshumba J et al (2019) Penetration of CD8+ cytotoxic T cells into large target, tissue cysts of *Toxoplasma gondii*, leads to its elimination. *Am J Pathol* 189:1594–1607. <https://doi.org/10.1016/J.AJPATH.2019.04.018>
- Trotta F (2019) Metal organic frameworks in medicine. *Acta Sci Pharm Sci* 3:107–109
- Wei H, Wei S, Lindsay D, Peng H (2015) A systematic review and meta-analysis of the efficacy of anti-*Toxoplasma gondii* medicines in humans. *PLoS ONE* 10:1–12. <https://doi.org/10.1371/journal.pone.0138204>



- Xing L, Dawei C, Liping X, Rongqing Z (2003) Oral colon-specific drug delivery for bee venom peptide: Development of a coated calcium alginate gel beads-entrapped liposome. *J Control Release* 93:293–300. <https://doi.org/10.1016/j.jconrel.2003.08.019>
- Yefet E, Schwartz N, Chazan B et al (2018) The safety of quinolones and fluoroquinolones in pregnancy: a meta-analysis. *BJOG* 125:1069–1076. <https://doi.org/10.1111/1471-0528.15119>
- Zheng Y, Zhao Y, Bai M et al (2022) Metal-organic frameworks as a therapeutic strategy for lung diseases. *J Mater Chem B* 10:5666–5695. <https://doi.org/10.1039/D2TB00690A>
- Ziv A, Masarwa R, Perlman A et al (2018) Pregnancy outcomes following exposure to quinolone antibiotics - a systematic-review

and meta-analysis. *Pharm Res*. <https://doi.org/10.1007/S11095-018-2383-8>

**Publisher's Note** Springer Nature remains neutral with regard to jurisdictional claims in published maps and institutional affiliations.

Springer Nature or its licensor (e.g. a society or other partner) holds exclusive rights to this article under a publishing agreement with the author(s) or other rightsholder(s); author self-archiving of the accepted manuscript version of this article is solely governed by the terms of such publishing agreement and applicable law.